On Landau Theory and Symmetric Energy Landscapes for Phase Transitions

Kai Hormann
Department of Informatics
Clausthal University of Technology

Johannes Zimmer
Department of Mathematical Sciences
University of Bath

Abstract

The aim of this presentation is the development of a general approach for modelling the global complex energy landscapes of phase transitions. For the sake of clarity and brevity the exposition is restricted to martensitic phase transition (i.e., diffusionless phase transitions in crystalline solids). The methods, however, are more broadly applicable. Explicit energy functions are derived for the cubic-to-tetragonal phase transition, where data is fitted for InTl. Another example is given for the cubic-to-monoclinic transition in CuZnAl. The resulting energies are defined globally, in a piecewise manner. We use splines that are twice continuously differentiable to ensure sufficient smoothness. The modular (piecewise) technique advocated here allows for modelling elastic moduli, energy barriers and other characteristics independently of each other.

1 Introduction

The central concern of this article is the explicit construction of nonconvex energy functions, which describe the complex energetic landscape of a material undergoing phase transitions. Ideas are laid out for symmetry-breaking martensitic transformations occurring in active crystalline materials, such as shape-memory alloys. The methods described are applicable to many other situations involving symmetry breaking, and are effective both for first and second order transitions.

One manner of modelling martensitic phase transitions occurs in the framework of nonlinear thermoelasticity. Here, phase transitions can be described as changes in the Helmholtz free energy density. This is a traditional method dating back to Landau [1967]. The Landau theory of phase transitions is described in great detail by Tolédano and Tolédano [1987]. Typically, the energy function is assumed to be analytic and therefore expanded into a power series. In practice, one often constructs energy functions which are polynomial in the components of the strain. Precisely, this approach has been applied to martensitic transformations in crystalline solids [Falk and Konopka, 1990; Fadda et al., 2002]. Using polynomials is one common way of modelling multi-well energies; another is to use piecewise quadratic functions. In the latter approach, one typically defines quadratic wells centred at the stable phases, and defines the energy as the minimum of these quadratic expressions. The energy is then continuous, while the stress tensors exhibits jumps.

Polynomials of the lowest feasible order often lead to unsatisfactory results, in particular, in several space dimensions. Often, they do not provide enough freedom to fit all elastic moduli. For example, Fadda et al. [2002] use this approach to derive an energy for Zirconia, which has a tetragonal-orthorhombic (orthoI)-monoclinic (t-o-m) triple point. They show that it is impossible to fit all elastic moduli of the tetragonal and the monoclinic phase accurately within this framework. Two elastic moduli of the monoclinic phase, C_{25}^{m} and C_{35}^{m}, are too high by an order of magnitude and by about 150% respectively, both with regard to the closest available experimental and theoretical data. As demonstrated by Dondl and Zimmer [2004], a lowest order polynomial can also result in an energy barrier that is extremely shallow. In numerical investigations [Dondl and Zimmer, 2004], the lowest-order polynomial energy fails to exhibit clearly distinguishable phases.

To determine the energy barrier correctly, Gooding et al. [1991] use invariant polynomials of higher order. Whilst neatly avoiding unrealistic estimates for the thermal activation energy, which are frequently obtained with the minimal set of order parameters, their method is technically difficult and results in steeply growing energy functions. Also, it then becomes more challenging to prove that the energy function has no other minima than the prescribed ones.

For the cubic-to-tetragonal transformation in InTl, Ericksen [1986] and James [1988] derive a temperature-dependent, rational energy function that interpolates the energy wells. Their ansatz is remarkably well suited for fitting the elastic moduli and approximates most elastic moduli with high precision. However, this energy function yields $C_{44}^{\mathrm{t}} = C_{55}^{\mathrm{t}} = C_{66}^{\mathrm{t}}$, which results in a value for C_{66}^{t} that is too small by about 46%. See Section 4 for the interpolated data, where an energy is derived that accurately interpolates all elastic moduli.

Zimmer [2004] describes an alternative approach to derive energy functions with a given symmetry. The method is briefly sketched in Section 2. These ideas are used by Dondl and Zimmer [2004] to derive a phenomenological isothermal energy density for Zirconia using piecewise functions. They demonstrate that an accurate fitting of the energy to given values for the elastic moduli of the different phases (tetragonal, orthorhombic, and monoclinic) becomes a relatively simple task. However, Dondl and Zimmer [2004] acknowledge that the flexibility gained by adopting the piecewise approach comes at a price. They use an energy function which is only C^1 and excludes temperature effects. In addition, their technique in principle carries a substantial number of degrees of freedom.

The aim of this paper is to demonstrate that, as conjectured by Dondl and Zimmer [2004], the use of splines avoids the aforementioned problems. Indeed, the derivation of a phenomenologically correct energy function then becomes rather straightforward. In order to guarantee a sufficiently smooth result and still have enough flexibility to meet all constraints, our construction is based on piecewise cubic, C^2-continuous splines. We take additional care to avoid the arbitrary nature of choosing parameters by selecting the spline spaces such that all parameters are uniquely determined by the constraints. For the wealth of data obtainable from *ab initio* calculations, the methods presented in this paper are a natural way of interpolating and deriving energy functions; invariant polynomials offer much less variety for accommodating experimental or theoretical data.

The Landau-Ericksen theory [Landau, 1967; Ericksen, 1980] is commonly used for a *local* analysis of the energy in the vicinity of bifurcation points only. Polynomials have proven to be an appropriate choice. Here, we define the energy function with splines, a new proposal that seems to be a natural extension of the original ideas put forward by Landau. Thus, we are able to reconstruct the *global* energy picture.

Indeed, the assumption of analyticity often associated with Landau theory might be too restrictive for far-from-equilibrium situations. Specifically, we wish to highlight recent work by Tröster et al. [2005] on the ϕ^4 model; by means of Wang-Landau simulations, these authors discover plateaus in the energetic landscape far from equilibrium and motivate these findings. They point out the inadequacy of a polynomial interpolation in this context. The ideas put forward here might be a natural approach to derive explicit representations of energy landscapes obtained from simulations over a wide range of parameters. It is plausible that the assumption of analyticity of the energy is too rigid to capture the far-from-equilibrium situation correctly; evidence is collected by Tröster et al. [2005]. If indeed analyticity cannot be assumed for certain parameter ranges, then the methods proposed here seem to be a suitable extension of Landau's original ideas.

The article is further organised as follows: in Section 2, methods from invariant theory are recalled and applied to the bifurcations from a cubic high-symmetry phase. In Section 3, a suitable class of splines is introduced that allows for a more flexible construction of energetic landscapes, as compared with approaches using polynomials. Applications to the cubic-to-tetragonal transition in InTl and the cubic-to-monoclinic transition in CuZnAl are given in Section 4. Explicit energies interpolating the available data, such as elastic moduli, are presented and listed explicitly in Appendix A and Appendix B. We close with a discussion in Section 5.

2 Tools from Invariant Theory

It is expedient to present some background aspects here, so that this article may remain self-explanatory. These aspects are also discussed in detail elsewhere [Zimmer, 2004].

As usual, we study phase transformations in a continuum framework by invoking the Cauchy-Born rule [Ericksen, 1984]. Let $\Omega \subset \mathbb{R}^3$ denote the reference configuration. The deformation of the crystal is given by $y(x)$. The displacement is defined as $u(x) := y(x) - x$. The deformation gradient $F_{jk} := \frac{\partial y_j}{\partial x_k}$ serves, according to the Cauchy-Born rule, as a measure of the deformation of the lattice. The axiom of frame indifference and the polar decomposition imply that the energy function can be written as a function of $C := F^T F$. Equivalently, it can be expressed in terms of the Green-St. Venant strain tensor $E := \frac{1}{2}(F^T F - \mathrm{Id}) \in \mathrm{Sym}(3, \mathbb{R})$. Here, $\mathrm{Sym}(3, \mathbb{R})$ is the space of symmetric real matrices in three space dimensions. The Green-St. Venant tensor E will be written as

$$E = \begin{pmatrix} e_1 & \frac{1}{2}e_6 & \frac{1}{2}e_5 \\ \frac{1}{2}e_6 & e_2 & \frac{1}{2}e_4 \\ \frac{1}{2}e_5 & \frac{1}{2}e_4 & e_3 \end{pmatrix}$$

with $e_j \in \mathbb{R}$ for $j = 1, \ldots, 6$.

The energy has to be invariant under the action of the point group $\mathcal{P}$ of the high-symmetry phase. For a cubic parent phase, $\mathcal{P}$ is the group of orientation-preserving mappings of the cube to itself. In formulas, the action of $P \in \mathcal{P}$ on $E \in \mathrm{Sym}(3, \mathbb{R})$ reads

$$\begin{aligned} \mathcal{P} \times \mathrm{Sym}(3, \mathbb{R}) &\to \mathrm{Sym}(3, \mathbb{R}) \\ (P, E) &\mapsto PEP^{-1}. \end{aligned}$$

Note that PEP^{-1} is symmetric since $P^* = P^{-1}$. Therefore, this defines an action of $\mathcal{P}$ on $\mathrm{Sym}(3, \mathbb{R})$.

The next step is to find invariant polynomials in $e_1, \ldots, e_6$ under the action of the high symmetry point group. The cornerstone for achieving this is the following theorem of Hilbert.

Theorem 1 (Hilbert). *The ring of invariant polynomials of a finite matrix group $\mathcal{P}$ is finitely generated. That is, there are finitely many invariant polynomials $\rho_1, \ldots, \rho_k$, such that every invariant polynomial p can be written as $p = \Pi(\rho_1, \ldots, \rho_k)$, where Π is a polynomial in k variables. In this case, $\{\rho_1, \ldots, \rho_k\}$ is a* Hilbert basis *or* integrity basis.

A proof of this theorem can be found, e.g., in Sturmfels [1993, Theorem 2.1.3]. For the different crystal classes, such a basis has been derived by Smith and Rivlin [1958]. An invariant basis can easily be computed automatically, for example, with Singular [Greuel et al., 2001].

So far, we considered only polynomial invariants. More generally, a set of invariants $\{f_1, \ldots, f_k\}$ is a *functional basis* if every invariant f can be expressed as a function of $f_1, \ldots, f_k$. Every Hilbert basis is a functional basis [Wineman and Pipkin, 1964, Sections 5 & 6]. In this article, splines defined as functions of a Hilbert basis are constructed to serve as a phenomenological model of the energy landscape under consideration. In principle, the same framework can be applied to a functional basis, which may not be polynomial; this might result in an even simpler form of the energy. The choice of the basis influences the ease of the construction. Even within the realm of polynomials, there are bases with a different number of elements. The Hilbert basis chosen here has the advantage that a geometric interpretation of the location of the phases can be given [Zimmer, 2004].

Zimmer [2004] computed the following basis for the cubic symmetry group. Note that here the labelling is different. To transfer to the notation we use here, it is necessary to apply the permutation (e_4, e_6, e_5) to the invariants given by Zimmer [2004].

Theorem 2 (Zimmer [2004]). *The ring of invariant polynomials is generated by*

$$\begin{aligned}
\rho_1 &:= e_1 + e_2 + e_3,\\
\rho_2 &:= e_1^2 + e_2^2 + e_3^2,\\
\rho_3 &:= e_4^2 + e_5^2 + e_6^2,\\
\rho_4 &:= e_1^3 + e_2^3 + e_3^3,\\
\rho_5 &:= e_4 e_5 e_6,\\
\rho_6 &:= e_4^4 + e_5^4 + e_6^4,\\
\rho_7 &:= 1,\\
\rho_8 &:= e_1 e_6^2 + e_2 e_6^2 + e_2 e_4^2 + e_3 e_4^2 + e_1 e_5^2 + e_3 e_5^2,\\
\rho_9 &:= e_1^2 e_6^2 + e_2^2 e_6^2 + e_2^2 e_4^2 + e_3^2 e_4^2 + e_1^2 e_5^2 + e_3^2 e_5^2,\\
\rho_{10} &:= e_1 e_6^4 + e_2 e_6^4 + e_2 e_4^4 + e_3 e_4^4 + e_1 e_5^4 + e_3 e_5^4,\\
\rho_{11} &:= e_1^2 e_6^4 + e_2^2 e_6^4 + e_2^2 e_4^4 + e_3^2 e_4^4 + e_1^2 e_5^4 + e_3^2 e_5^4,\\
\rho_{12} &:= e_1^2 e_2 e_6^4 e_4^2 + e_2 e_3^2 e_6^2 e_4^4 + e_1 e_2^2 e_6^4 e_5^2 + e_2^2 e_3 e_4^4 e_5^2 + e_1 e_3^2 e_6^2 e_5^4 + e_1^2 e_3 e_4^2 e_5^4.
\end{aligned}$$

This basis enjoys an advantageous algebraic structure, since it is a Cohen-Macaulay basis. See [Zimmer, 2004] for more details.

The map $\rho\colon \mathbb{R}^6 \to \mathbb{R}^{12}, (e_1, \ldots, e_6) \mapsto (\rho_1(e_1, \ldots, e_6), \ldots, \rho_{12}(e_1, \ldots, e_6))$ is called the *Hilbert map*. To estimate its relevance, one more definition is called for: the ($\mathcal{P}$-)*orbit* of $e \in \mathbb{R}^6$ is the set $\mathcal{P}e := \{Pe \mid P \in \mathcal{P}\}$. The set of all orbits is denoted as the *orbit space*. One can easily see that a bijection between the image $\rho(\mathbb{R}^6)$ and the orbit space exists [Rumberger, 1997; Zimmer, 2004, Lemma 1].

Every function $W(e) := \bar{W}(\rho(e))$ will automatically have the correct symmetries. One needs to determine $\bar{W}$ in such a way that it has minima for the stable phases and interpolates the available experimental data. It is known that orbit spaces can be defined by a set of inequalities [Procesi and Schwarz, 1985]. Zimmer [2004] gives a specialised version using projections to $\rho_1, \ldots, \rho_6$.

Proposition 3 (Zimmer [2004]). *For the action of $\mathcal{P}$ reduced to the off-diagonals e_4, e_5, e_6, a Hilbert basis is given by*

$$\begin{aligned}
\rho_1^{\mathrm{o}}(e_4, e_5, e_6) &:= \rho_3(e_4, e_5, e_6) = e_4^2 + e_5^2 + e_6^2,\\
\rho_2^{\mathrm{o}}(e_4, e_5, e_6) &:= \rho_5(e_4, e_5, e_6) = e_4 e_5 e_6,\\
\rho_3^{\mathrm{o}}(e_4, e_5, e_6) &:= \rho_6(e_4, e_5, e_6) = e_4^4 + e_5^4 + e_6^4.
\end{aligned}$$

For this Hilbert map, the image of $\mathrm{Sym}(3, \mathbb{R})^+$*, the set of symmetric matrices with positive determinant, in the orbit space is characterised by the inequalities*

$$\begin{aligned}
\rho_1^{\mathrm{o}} &\geq 0,\\
\rho_3^{\mathrm{o}} &\leq \rho_1^{\mathrm{o}2},\\
\rho_1^{\mathrm{o}6} - 20\rho_1^{\mathrm{o}3}\rho_2^{\mathrm{o}2} - 4\rho_1^{\mathrm{o}4}\rho_3^{\mathrm{o}} + 36\rho_1^{\mathrm{o}}\rho_2^{\mathrm{o}3}\rho_3^{\mathrm{o}} + 5\rho_1^{\mathrm{o}2}\rho_3^{\mathrm{o}2} + 108\rho_2^{\mathrm{o}4} - 2\rho_3^{\mathrm{o}3} &\leq 0.
\end{aligned}$$

A similar characterisation holds for the diagonal elements e_1, e_2, e_3. However, it turns out to be convenient to introduce a change of variables first. We follow Zimmer [2004] in defining

$$\begin{aligned}
s(e_1, e_2, e_3) &:= \tfrac{1}{\sqrt{3}}(e_1 + e_2 + e_3),\\
t(e_1, e_2, e_3) &:= \tfrac{1}{\sqrt{2}}(e_1 - e_2),\\
u(e_1, e_2, e_3) &:= \sqrt{\tfrac{2}{3}}\left(\tfrac{1}{2}e_1 + \tfrac{1}{2}e_2 - e_3\right).
\end{aligned}$$

Proposition 4 (Zimmer [2004]). *For the action of $\mathcal{P}$ reduced to the diagonals $s(e_1, e_2, e_3)$, $t(e_1, e_2, e_3)$, $u(e_1, e_2, e_3)$, a Hilbert basis is given by*

$$\tilde{\rho}_1^{\mathrm{d}}(s,t,u) := s = \tfrac{1}{\sqrt{3}}(e_1 + e_2 + e_3),$$

$$\tilde{\rho}_2^{\mathrm{d}}(s,t,u) := t^2 + u^2,$$

$$\tilde{\rho}_3^{\mathrm{d}}(s,t,u) := \tfrac{3}{\sqrt{2}}t^2u - \tfrac{1}{\sqrt{2}}u^3.$$

For this Hilbert map, the image of $\mathrm{Sym}(3,\mathbb{R})^+$ in the orbit space is characterised by the inequalities

$$\tilde{\rho}_2^{\mathrm{d}} \geq 0,$$

$$|\tilde{\rho}_3^{\mathrm{d}}| \leq \sqrt{\tfrac{1}{2}(\tilde{\rho}_2^{\mathrm{d}})^3}.$$

3 Tools from Geometric Modelling

It is well known that polynomial interpolation can lead to unwanted oscillations, if the interpolation points are not chosen properly. Therefore, piecewise polynomials have largely replaced the use of polynomials in many applications. In particular, the theory of B-splines gives rise to a powerful representation of piecewise polynomial functions that has become the de-facto standard of today's Computer-Aided Design (CAD) systems. We now give a brief overview of the definition and the properties of B-splines and refer to Schumaker [1993], de Boor [2001], Farin [2001] and Dierckx [1993] for more details.

Given the *knot vector* $\bar{t} = (t_i)_{i\in\mathbb{Z}}$ with $t_i < t_{i+1}$, the *normalised B-spline basis functions* $N_i^k = N_i^{\bar{t},k}$ of degree k over $\bar{t}$ are defined by the following recursion:

$$N_i^0(u) := \begin{cases} 1 & \text{if } u \in [t_i, t_{i+1}[, \\ 0 & \text{otherwise,} \end{cases}$$

$$N_i^j(u) := \frac{u - t_i}{t_{i+j} - t_i} N_i^{j-1}(u) + \frac{t_{i+j+1} - u}{t_{i+j+1} - t_{i+1}} N_{i+1}^{j-1}(u), \qquad j > 0.$$

The functions N_i^k are polynomial of degree k on each interval $[t_i, t_{i+1}[$ and have a number of interesting properties:

1. *Continuity:* N_i^k is C^{k-1}-continuous,
2. *Positivity:* $N_i^k(u) \geq 0$,
3. *Local support:* $N_i^k(u) = 0$, $u \notin [t_i, t_{i+k+1}[$,
4. *Partition of unity:* $\sum_{i\in\mathbb{Z}} N_i^k(u) = 1$,
5. *Derivative:* $(N_i^k)'(u) = \frac{k}{t_{i+k} - t_i} N_i^{k-1}(u) - \frac{k}{t_{i+k+1} - t_{i+1}} N_{i+1}^{k-1}(u)$.

Furthermore, the functions N_i^k with $i = j, \ldots, m$ form a basis of all functions that are piecewise polynomial of degree k over $[t_{k+j}, t_{m+1}]$, and

$$f(u) = \sum_{i=j}^{m} c_i N_i^k(u)$$

is a *B-spline* with *control points* (or *de Boor points*) c_i. B-splines are called *uniform* if the knot vector is equidistantly spaced, $t_{i+1} - t_i = h$.

In many applications, cubic B-splines ($k = 3$) are used because, on the one hand, they are sufficiently often (twice) differentiable, but on the one hand they are relatively cheap to compute. Usually, B-splines are evaluated with the *de Boor algorithm*, but for uniform knot vectors a more efficient method can be applied. Namely, for a uniform knot vector $\bar{t} = (\ldots, t_0 - h, t_0, t_0 + h, t_0 + 2h, \ldots)$ the B-spline functions differ by translation only, $N_{i+j}^{\bar{t},k}(u) = N_i^{\bar{t},k}(u - hj)$, and the evaluation of any basis function can be reduced to evaluating the B-spline function N_0^k defined on the integer knot vector, $N_j^{\bar{t},k}(u) = N_0^k(\frac{u-t_0}{h} - j)$. For uniform cubic B-splines it is therefore advisable to use the explicit piecewise polynomial representation of N_0^3 over the knot vector $(0, 1, 2, 3, 4)$,

$$N_0^3(u) = \begin{cases} \frac{1}{6}u^3 & \text{if } u \in [0, 1[, \\ -\frac{1}{2}u^3 + 2u^2 - 2u + \frac{2}{3} & \text{if } u \in [1, 2], \\ N_0^3(4 - u) & \text{if } u \in]2, 4[, \\ 0 & \text{otherwise,} \end{cases} \tag{1}$$

and Horner's method for evaluation. Note that first and second order derivatives of uniform cubic B-splines can be computed efficiently in the same way.

4 Applications: Energies for InTl and CuZnAl

We apply the tools developed in the previous sections to two specific applications. First, an energy density for the cubic-to-tetragonal transition in InTl is derived that interpolates all available elastic moduli exactly. The second example is an energy density for the cubic-to-monoclinic transition in CuZnAl.

4.1 Cubic-to-tetragonal transition in InTl

We wish to derive a temperature-dependent energy function for the cubic-to-tetragonal transformation in InTl. A very prominent energy function for this transition is the Ericksen-James energy [Ericksen, 1986; James, 1988]; it fits all but one elastic moduli exactly. The modulus C_{66}^{t} is underestimated by about 46%. The construction of Ericksen and James is certainly ingenious. However, it is extremely difficult to modify their energy, for example, to fit C_{66}^{t}. We wish to show that the framework presented here makes the derivation of an energy matching all elastic moduli a relatively simple task. We are fortunate to be able to use the experimental data for InTl collected by James [1988].

As usual, the austenitic (cubic) phase will be taken as the reference configuration. Consequently, the cubic phase itself is characterised by $e_1 = \cdots = e_6 = 0$. The tetragonal phase is $e_1 = e_2 = -\epsilon/2$, $e_3 = \epsilon$, $e_4 = e_5 = e_6 = 0$. [Burkart and Read, 1953] give $\epsilon = 0.026$.

We fit the elastic moduli of pure cubic Tl. The values in GPa are [Hellwege and Hellwege, 1979]:

$\hat{C}_{11}^{\mathrm{c}}$	$\hat{C}_{44}^{\mathrm{c}}$	$\hat{C}_{12}^{\mathrm{c}}$
40.8	11.0	34.0

(2)

Here, Love's notation [Love, 1944, Note A] is used, for example $\hat{C}_{44} = C_{2323}$; recall that the remaining moduli for the cubic phase are given by the symmetries $\hat{C}_{11}^{\mathrm{c}} = \hat{C}_{22}^{\mathrm{c}} = \hat{C}_{33}^{\mathrm{c}}$, $\hat{C}_{12}^{\mathrm{c}} = \hat{C}_{13}^{\mathrm{c}} = \hat{C}_{23}^{\mathrm{c}}$, and $\hat{C}_{44}^{\mathrm{c}} = \hat{C}_{55}^{\mathrm{c}} = \hat{C}_{66}^{\mathrm{c}}$.

We follow James [1988] in fitting the elastic moduli for pure In. Hellwege and Hellwege [1979] give the following values (in GPa):

$\hat{C}_{11}^{\mathrm{t}}$	$\hat{C}_{33}^{\mathrm{t}}$	$\hat{C}_{44}^{\mathrm{t}}$	$\hat{C}_{66}^{\mathrm{t}}$	$\hat{C}_{12}^{\mathrm{t}}$	$\hat{C}_{13}^{\mathrm{t}}$
45.2	44.9	6.52	12.0	40.0	41.2

(3)

and $\hat{C}_{11}^{\mathrm{t}} = \hat{C}_{22}^{\mathrm{t}}$, $\hat{C}_{13}^{\mathrm{t}} = \hat{C}_{23}^{\mathrm{t}}$, $\hat{C}_{44}^{\mathrm{t}} = \hat{C}_{55}^{\mathrm{t}}$ due to the symmetries of a tetragonal phase.

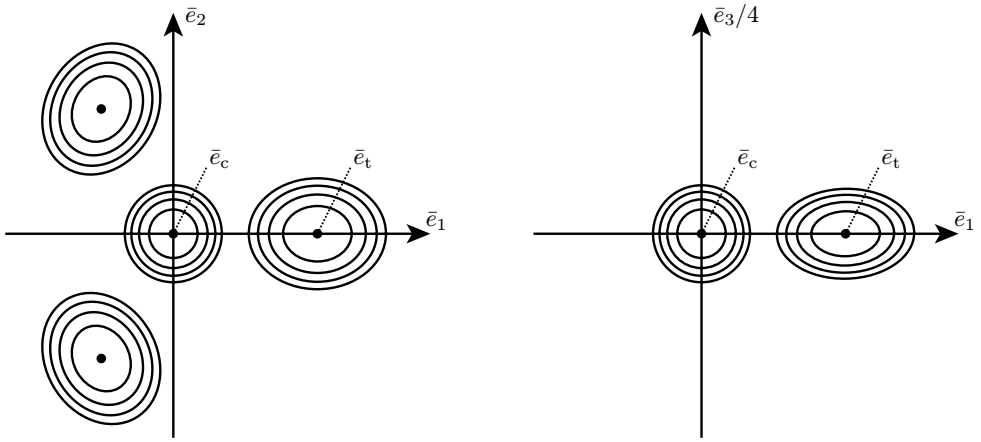

Figure 1: Local behaviour of the energy W_{d} around the cubic and tetragonal phases.

For most of the presentation, we will split the energy in two parts,

$$W(e_1, \dots, e_6) := W_{\mathrm{d}}(e_1, e_2, e_3) + W_{\mathrm{o}}(e_1, e_2, e_3, e_4, e_5, e_6),$$

and start by constructing W_{d}. Given that W_{d} is defined on the orbit space, it will automatically have the correct symmetry. We fit the elastic moduli for the cubic phase $e^{\mathrm{c}} := (0, 0, 0)$ and tetragonal phase $e^{\mathrm{t}} := (-\epsilon/2, -\epsilon/2, \epsilon)$ exactly by imposing the conditions

$$\mathrm{grad}(W_{\mathrm{d}})(e^{\mathrm{c}}) = 0, \qquad \mathrm{Hess}(W_{\mathrm{d}})(e^{\mathrm{c}}) = \hat{C}^{\mathrm{c}} := \begin{pmatrix} 40.8 & 34 & 34 \\ & 40.8 & 34 \\ & & 40.8 \end{pmatrix} \tag{4}$$

and

$$\mathrm{grad}(W_{\mathrm{d}})(e^{\mathrm{t}}) = 0, \qquad \mathrm{Hess}(W_{\mathrm{d}})(e^{\mathrm{t}}) = \hat{C}^{\mathrm{t}} := \begin{pmatrix} 45.2 & 40 & 41.2 \\ & 45.2 & 41.2 \\ & & 44.9 \end{pmatrix}. \tag{5}$$

Figure 1 may help to get a better intuition of the energy's local behaviour around the cubic and tetragonal phase by plotting for each phase the isolines of a local quadratic fit. Note that we used the coordinate system $\bar{e} = Me$ for this visualisation, where M is the orthogonal matrix

$$M := \frac{1}{\sqrt{6}} \begin{pmatrix} -1 & -1 & 2 \\ \sqrt{3} & -\sqrt{3} & 0 \\ \sqrt{2} & \sqrt{2} & \sqrt{2} \end{pmatrix}. \tag{6}$$

In this coordinate frame, all phases lie in the $\bar{e}_1$-$\bar{e}_2$-plane and the transformed elastic moduli are

$$\bar{C}^{\mathrm{c}} := M^{-T} \hat{C}^{\mathrm{c}} M^{-1} = \begin{pmatrix} 6.8 & 0 & 0 \\ & 6.8 & 0 \\ & & 108.8 \end{pmatrix} \tag{7}$$

and

$$\bar{C}^{\mathrm{t}} := M^{-T} \hat{C}^{\mathrm{t}} M^{-1} = \begin{pmatrix} 3.4 & 0 & 0.3\sqrt{2} \\ & 5.2 & 0 \\ & & 126.7 \end{pmatrix}. \tag{8}$$

We continue to construct W_d by composing the Hilbert map $\tilde{\rho}^\mathrm{d}$ given in Proposition 4 with the parameter transformation

$$\psi\colon (\tilde{\rho}_1^\mathrm{d}, \tilde{\rho}_2^\mathrm{d}, \tilde{\rho}_3^\mathrm{d}) \mapsto \big(\tilde{\rho}_1^\mathrm{d}, \tilde{\rho}_2^\mathrm{d}, \tilde{\rho}_3^\mathrm{d} - \tilde{\rho}_2^\mathrm{d}\sqrt{\tilde{\rho}_2^\mathrm{d}/2}\big).$$

The transformation ψ shifts the orbit space in $\tilde{\rho}_3^\mathrm{d}$-direction and maps the upper limit surface (compare Fig. 4 in Zimmer [2004]), which contains the tetragonal phase $\tilde{\rho}^\mathrm{d}(e^\mathrm{t})$, to the $\tilde{\rho}_1^\mathrm{d}$-$\tilde{\rho}_2^\mathrm{d}$-plane.

As mentioned in Section 2, the task now is to determine an appropriate function W_τ defined on the transformed orbit space $\tau := \psi \circ \tilde{\rho}^\mathrm{d}(\mathbb{R}^3)$, so that $W_\mathrm{d} := W_\tau \circ \tau$ behaves as expected at the cubic and tetragonal phases. The positions of the minima in the transformed orbit space are $\tau^\mathrm{c} := \tau(e^\mathrm{c}) = (0,0,0)$ and $\tau^\mathrm{t} := \tau(e^\mathrm{t}) = (0, 1.5\,\epsilon^2, 0)$. By the chain rule and the product rule, we have

$$\mathrm{grad}(W_\mathrm{d}) = \mathrm{grad}(W_\tau) \cdot J_\tau \tag{9}$$

and

$$\mathrm{Hess}(W_\mathrm{d}) = {J_\tau}^T \cdot \mathrm{Hess}(W_\tau) \cdot J_\tau + \mathrm{grad}(W_\tau) \cdot H_\tau$$

where $J_\tau = \left(\frac{\partial \tau_i}{\partial e_j}\right)_{ij}$ is the Jacobian and $H_\tau = (\mathrm{Hess}(\tau_i))_i$ is the Hessian of τ. A routine calculation shows that (4) and (5) hold if and only if W_τ meets the following constraints (entries $*$ have no influence and will be set to zero for the sake of simplicity):

$$\mathrm{grad}(W_\tau)(\tau^\mathrm{c}) = (0, 3.4, *), \qquad \mathrm{Hess}(W_\tau)(\tau^\mathrm{c}) = \begin{pmatrix} 108.8 & * & * \\ & * & * \\ & & * \end{pmatrix} \tag{10}$$

and

$$\mathrm{grad}(W_\tau)(\tau^\mathrm{t}) = (0, 0, -26\delta), \qquad \mathrm{Hess}(W_\tau)(\tau^\mathrm{t}) = \begin{pmatrix} 126.7 & 6.75\,\delta & * \\ & 860.625\,\delta^2 & * \\ & & * \end{pmatrix} \tag{11}$$

with $\delta := \frac{2\sqrt{3}}{135\epsilon} \approx 0.9869$.

Our ansatz is further to simplify the fitting process by reducing it to the construction of two univariate functions: a *path* α that deforms the τ_2-axis and a *profile* β along this path. We then define W_τ as

$$W_\tau(\tau_1, \tau_2, \tau_3) := \big(\tau_1 - \alpha(\tau_2)\big)^2 \Big(\omega_1 + (\omega_2 - \omega_1)\frac{\tau_2}{\tau_*}\Big) + \beta(\tau_2) - 26\delta\tau_3 \tag{12}$$

with $\tau_* := \tau_2(e^\mathrm{t}) = 1.5\,\epsilon^2$ and constants ω_1, ω_2.

To understand the idea behind this construction, let us assume $\alpha \equiv 0$ for a moment. Then, the first factor of the product in W_τ simply defines a parabola in τ_1 with its minimum at $\tau_1 = 0$. The second factor results in a linear variation of the width of this parabola along the τ_2-axis; the energy value at its minimum follows the profile curve β. The last term defines a linear increase in the negative τ_3-direction. Altogether, this construction is sufficient to fit all the constraints on W_τ except for the off-diagonal element in $\mathrm{Hess}(W_\tau)(\tau^\mathrm{t})$.

Letting the minimum of the parabola follow a general path $\alpha(\tau_2)$ gives an additional degree of freedom while maintaining the simple structure of W_τ; the energy still is a composition of univariate functions. If we now construct α and β such that

$$\alpha(0) = \alpha'(0) = \alpha''(0) = \alpha(\tau_*) = \alpha''(\tau_*) = 0, \qquad \beta(0) = \beta(\tau_*) = \beta'(\tau_*) = 0,$$

then it is easy to verify that (10) is fulfilled if we impose

$$\omega_1 = 54.4, \qquad \beta'(0) = 3.4.$$

Similarly, (11) holds if

$$\omega_2 = \mathrm{T}_{11}/2, \qquad \alpha'(\tau_*) = \mathrm{T}_{12}/\mathrm{T}_{11}, \qquad \beta''(\tau_*) = \mathrm{T}_{22} - (\mathrm{T}_{12})^2/\mathrm{T}_{11},$$

where the T_{jk} are the (non-zero) entries of $\mathrm{Hess}(W_\tau)(\tau^\mathrm{t})$ in Equation (11).

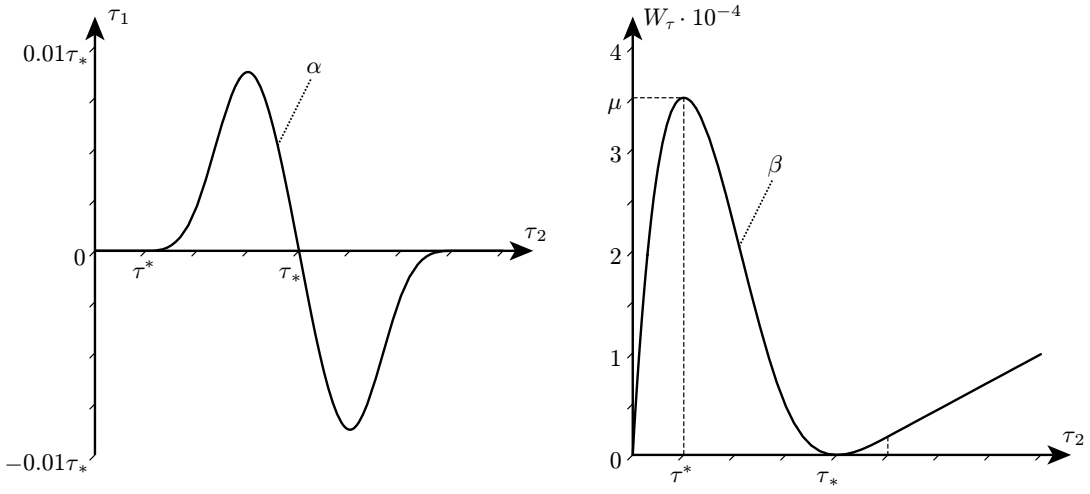

Figure 2: Path α (left) and profile β (right).

Another advantage of this approach that decomposes W_τ into a path and a profile is that we can easily add constraints to specify position and height of the energy saddle between the different phases. For example,

$$\alpha(\tau^*) = \alpha'(\tau^*) = \alpha''(\tau^*) = 0, \qquad \beta(\tau^*) = \mu, \qquad \beta'(\tau^*) = 0, \qquad \beta''(\tau^*) < 0$$

with $\tau^* := \tau_2(\frac{e^c+e^t}{2}) = \tau_*/4$ are sufficient conditions for W to have a saddle of height μ halfway between the cubic and the tetragonal phases.

Although it is possible to model both α and β as polynomials, we decided to resort to cubic B-splines in order to avoid oscillations and in particular unwanted minima for β. We keep the setting as simple as possible by using the uniform knot vector $\bar{t} = (t_i)_{i\in\mathbb{Z}}$ with $t_i = i\tau^*$, so that all conditions on the splines

$$\alpha(u) := \sum_{i=-3}^{3} a_i N_i^3(u) \qquad \text{and} \qquad \beta(u) := \sum_{i=-3}^{4} b_i N_i^3(u)$$

fall on a knot and involve only three basis functions. The coefficients a_i and b_i are uniquely determined by these conditions and can be found by solving the corresponding systems of linear equations. Note that we added one additional degree of freedom to β to obtain $\beta''(t_5) = 0$, so that we can extend $\beta(u)$ linearly and with C^2-continuity for $u > t_5$.

A further analysis shows that β does not have other local minima than the one at τ_* as long as μ is between $2.873 \cdot 10^{-4}$ and $5.8357 \cdot 10^{-4}$. We decided to set $\mu := 3.5 \cdot 10^{-4}$. Figure 2 plots the resulting functions α and β.

This construction defines the energy W_τ from Equation (12) in orbit space such that the energy $W_\mathrm{d} = W_\tau \circ \tau$ has the correct minima in E-space. In order to ensure that W_d has no local minima other than the prescribed ones, let us inspect the gradient of W_d. Note that $\operatorname{grad}(W_\mathrm{d}) = (0,0,0)$ is not equivalent to $\operatorname{grad}(W_\tau) = (0,0,0)$ as the matrix J_τ in Equation (9) does not necessarily have full rank; more precisely, it is singular at all points that lie on the boundary of the orbit space. And in fact, it is easy to see that the gradient of W_τ never vanishes in orbit space, because $\frac{\partial W_\tau}{\partial \tau_3} = -26\delta$. However, a careful analysis reveals that the necessary condition for a vanishing gradient in E-space is

$$\begin{aligned}
&\operatorname{grad}(W_\tau) = (0,*,*) && \text{for } \tau_2 = 0,\ \tau_3 = 0 && (\tau_1\text{-axis}),\\
&\operatorname{grad}(W_\tau) = (0,0,*) && \text{for } \tau_2 > 0,\ \tau_3 = 0 && (\text{upper limit surface}),\\
&\operatorname{grad}(W_\tau) = \lambda\,(0, 3\sqrt{\tau_2/2}, 1) && \text{for } \tau_2 > 0,\ \tau_3 = -\sqrt{2(\tau_2)^3} && (\text{lower limit surface}),
\end{aligned}$$

with some arbitrary scaling factor λ in the last case.

Along the τ_1-axis, this condition holds only at the cubic phase τ^{c} and on the upper limit surface at the tetragonal phase τ^{t} and the saddle $(0, \tau^*, 0)$ only, as expected. On the lower limit surface, the condition is fulfilled if and only if

$$\tau_1 = \alpha(\tau_2) \qquad \text{and} \qquad \beta'(\tau_2) = -78\delta\sqrt{\tau_2/2},$$

which does not happen in our construction as long as the saddle height μ is set to a value smaller than $4.1314 \cdot 10^{-4}$. Otherwise, the energy W_{d} would have other stationary points than the expected ones, but they turn out to be saddle points, rather than local minima.

To fit the remaining moduli for the off-diagonal elements we use the ansatz

$$W_{\mathrm{o}} := \lambda_1 \cdot (\rho_2\rho_3 - \rho_9) + \lambda_2(\rho_2) \cdot \rho_3, \tag{13}$$

where λ_1 is a constant, $\lambda_2 \colon \mathbb{R} \to \mathbb{R}$ is a profile curve similar to β in the construction of W_ρ, and ρ_2, ρ_3, ρ_9 are the invariant polynomials given in Theorem 2. It is then easy to verify that the desired properties

$$\operatorname{grad}(W_{\mathrm{o}})(e^{\mathrm{c}}) = 0, \qquad \operatorname{Hess}(W_{\mathrm{o}})(e^{\mathrm{c}}) = \operatorname{diag}(0,0,0,11,11,11)$$

and

$$\operatorname{grad}(W_{\mathrm{o}})(e^{\mathrm{t}}) = 0, \qquad \operatorname{Hess}(W_{\mathrm{o}})(e^{\mathrm{t}}) = \operatorname{diag}(0,0,0,6.52,6.52,12)$$

are fulfilled if and only if

$$\lambda_1 = \frac{274}{75\,\epsilon^2} = 5548.5\,\delta^2$$

and

$$\lambda_2(0) = \lambda_2(\rho_2(e^{\mathrm{c}})) = \frac{11}{2},$$
$$\lambda_2(1.5\,\epsilon^2) = \lambda_2(\rho_2(e^{\mathrm{t}})) = \frac{176}{75}.$$

We can achieve this, for example, by letting λ_2 be the quadratic function

$$\lambda_2(u) := \frac{946}{675\,\epsilon^4}\big(u - 1.5\,\epsilon^2\big)^2 + \frac{176}{75}$$

which further attains its minimum at the tetragonal phase. By this construction, the energy W_{o} from (13) is non-negative everywhere and equal to zero if and only if $e_4 = e_5 = e_6 = 0$. As it can also be shown that the gradient of W_{o} vanishes if and only if $e_4 = e_5 = e_6 = 0$, we can safely add it to the energy W_{d}, resulting in the overall energy $W = W_{\mathrm{d}} + W_{\mathrm{o}}$, without introducing additional stationary points.

We also need to take into account the effect of stress on the transformation temperature. For the moment, we denote $\tilde{W}$ when regarding the energy as a function of the deformation gradient F and the temperature θ to distinguish it from the energy W regarded as a function of $C = F^T F$ and the temperature θ. We consider the Clausius-Clapeyron equation

$$-\frac{\mathrm{d}T}{\mathrm{d}\theta}\left(F_2(\theta) - F_1(\theta)\right) = \frac{\partial\tilde{W}}{\partial\theta}\left(F_1(\theta), \theta\right) - \frac{\partial\tilde{W}}{\partial\theta}\left(F_2(\theta), \theta\right). \tag{14}$$

This is an approximation, as the Clausius-Clapeyron equation is expected to describe the global minimum of the energy only. Here, the material exhibits hysteretic effects, corresponding to a wiggly energy landscape. It is thus not clear whether the available experimental data describes the ground state or a local minimum. The hysteresis loop in the temperature-stress diagram is reasonably small (e.g., for tensile loading in Indium-Thallium about 5°C at a transformation temperature at around 73°C). Of course, it would be straightforward to fit experimental data guaranteed to describe the ground state.

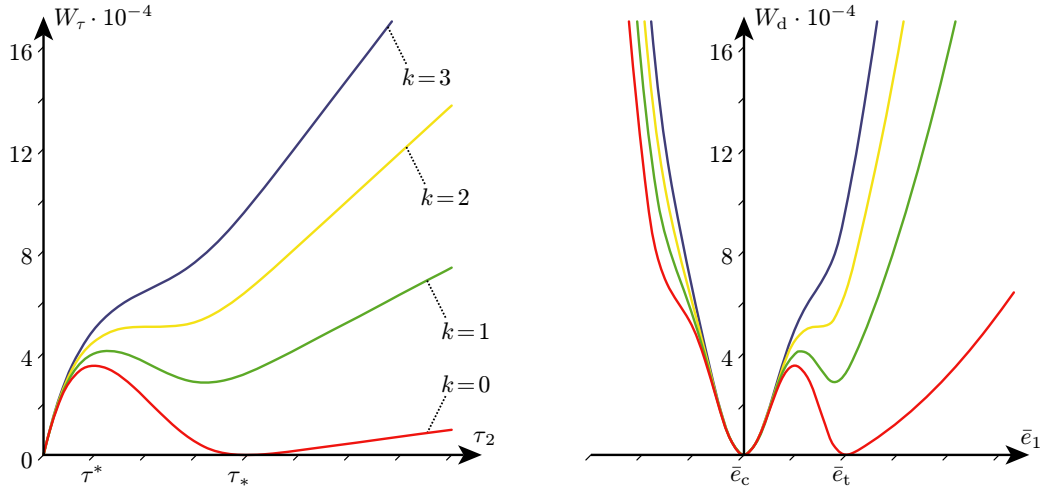

Figure 3: Profile $\beta(u,\theta)$ (left) and energy in E-space, restricted to the $\bar{e}_1$-axis (right). Both plots show the behaviour for different temperatures $\theta_c + \frac{k}{2}\theta_*$. The plot for $k = 2$ corresponds to the temperature at which the tetragonal minimum vanishes ($\approx 45.34°\mathrm{C}$).

James [1988] examines a dead loading device for a shear experiment with

$$T(\theta) = \begin{pmatrix} 0 & 0 & 0 \\ 0 & 0 & 0 \\ 0 & 0 & \sigma(\theta) \end{pmatrix}.$$

For this experiment, we evaluate the Clausius-Clapeyron equation (14) at $\theta = \theta_c = 25°\mathrm{C}$, the stable equilibrium configurations $F_1(\theta_c) = \mathrm{Id}$ for the cubic phase and $F_2(\theta_c) = \mathrm{diag}(\sqrt{1-\epsilon}, \sqrt{1-\epsilon}, \sqrt{1+2\epsilon})$ for the tetragonal phase. With the approximation $\sqrt{1+2\epsilon} \approx 1+\epsilon$, Equation (14) becomes

$$-\sigma'(\theta_c)\epsilon = \frac{\partial W}{\partial \theta}\left(C_1(\theta), \theta\right) - \frac{\partial W}{\partial \theta}\left(C_2(\theta), \theta\right). \tag{15}$$

We still follow the discussion in James [1988] in assuming

$$\sigma'(\theta_c) = 323 \frac{\mathrm{g}}{\mathrm{cm}^2\ {}^\circ\mathrm{C}} \approx 3.17 \cdot 10^4 \frac{\mathrm{Pa}}{{}^\circ\mathrm{C}}. \tag{16}$$

Since $W(C_1) = 0$, Equations (15)–(16) tell us the rate at which the martensitic well vanishes at higher temperatures.

This behaviour can be modelled by replacing the path $\beta(u)$ with a temperature-dependent path $\beta(u,\theta)$ that reproduces $\beta(u)$ for $\theta = \theta_c$ and fulfils

$$\frac{\partial}{\partial \theta}\beta(\rho_*, \theta_c) = \sigma'(\theta_c). \tag{17}$$

To keep everything as simple as possible, we decided to define $\beta(u,\theta)$ as a linear blend between $\beta(u)$ and the linear function $\tilde{\beta}(u) = \beta'(0)u$, so as smoothly to blend out the minimum of the tetragonal phase. Thus,

$$\beta(u,\theta) := \frac{\theta^* - \theta}{\theta^* - \theta_c}\beta(u) + \frac{\theta - \theta_c}{\theta^* - \theta_c}\tilde{\beta}(u)$$

with $\theta^* := \beta'(0)\rho_*/\sigma'(\theta_c) + \theta_c$ so that Equation (17) holds. Note that $\tilde{\beta}(u)$ can be considered a cubic spline with coefficients $\tilde{b}_i := t_{i+2}\beta'(0)$ and therefore also $\beta(u,\theta)$ is a cubic spline, with linearly varying coefficients

$$b_i(\theta) := \frac{\theta^* - \theta}{\theta^* - \theta_c} b_i + \frac{\theta - \theta_c}{\theta^* - \theta_c}\tilde{b}_i.$$

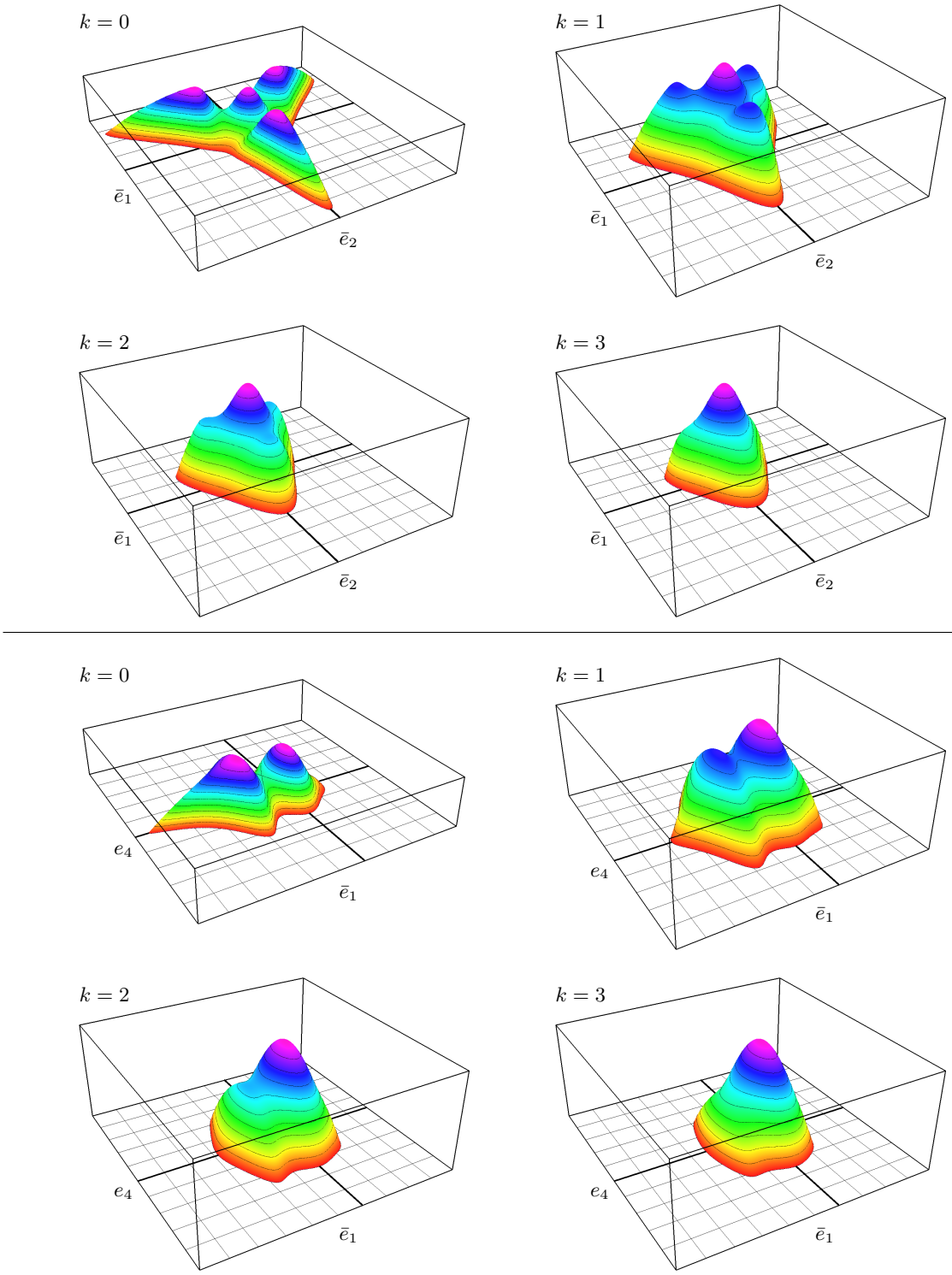

Figure 4: Energy in E-space, restricted to the $\bar{e}_1$-$\bar{e}_2$-plane (top) and the $\bar{e}_1$-e_4-plane (bottom), for different temperatures $\theta_c + \frac{k}{2}\theta_*$; compare Figure 3. Note that we plot the negative energy to obtain a better view of the minima. For $k = 0$ the plot shows the energy between 0 and 2μ, for all other k the energy ranges from 0 to 4μ with $\mu = 3.5 \cdot 10^{-4}$.

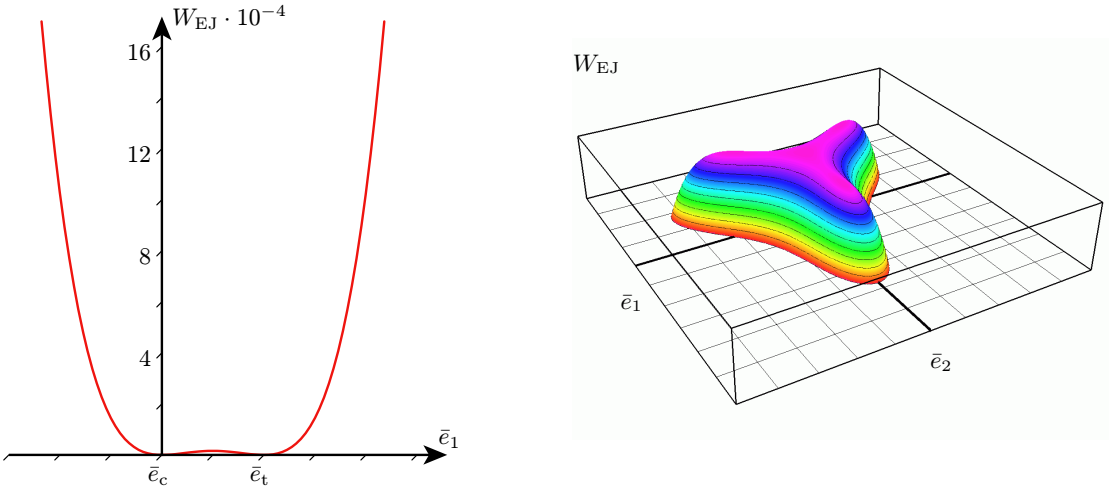

Figure 5: Ericksen-James energy in E-space, restricted to the $\bar{e}_1$-axis (left) and the $\bar{e}_1$-$\bar{e}_2$-plane (right). The plots correspond to the plots of our energy in Figure 3 (right) and Figure 4 (top left). It is noticeable that the wells are less pronounced in the Ericksen-James energy.

Figures 3 and 4 show the path as well as the resulting energy for different values of θ. Analysing the quadratic spline $\frac{\partial}{\partial u}\beta(u,\theta)$, we find it to be positive (and thus β to be monotone) for $\theta - \theta_c \geq \theta_* \approx 20.34°\mathrm{C}$. The minimum vanishes at $u \approx 0.523\rho_*$ which translates to approximately $0.723e^{\mathrm{t}}$ in E-space. Of course, this is not the only way to construct a temperature-dependent energy, but the idea itself can easily be extended if more data is available. A recapitulating summary of our construction is given in Appendix A.

We conclude this subsection by comparing the energy derived here with the well-known Ericksen-James energy [Ericksen, 1986; James, 1988]. This energy, as a function of $C = F^T F$, is defined as

$$W_{\mathrm{EJ}}(C) := bJ + cK + dJ^2 + eL + f(\mathrm{tr}(C) - 3)^2, \tag{18}$$

where

$$J := \tfrac{1}{6}\big((F-1)^2 + (G-1)^2 + (H-1)^2\big),$$
$$K := \tfrac{1}{2}(F-1)(G-1)(H-1),$$
$$L := {C_{12}}^2 + {C_{23}}^2 + {C_{13}}^2,$$

and

$$F := \frac{3C_{11}}{\mathrm{tr}(C)}, \qquad G := \frac{3C_{22}}{\mathrm{tr}(C)}, \qquad H := \frac{3C_{33}}{\mathrm{tr}(C)},$$

with

$$\mathrm{tr}(C) := C_{11} + C_{22} + C_{33}.$$

We use the value $b := 0.38 + 1.22 \cdot 10^{-3} \cdot (\theta - 25°\mathrm{C})$ for the temperature-dependent term and the constants

$$c := -29.23, \qquad d := 562.13, \qquad e := 3.26, \qquad f := 5.25$$

(temperature in °C, moduli in GPa). The value for f differs from the one found in the literature, but it yields a better approximation of the elastic moduli, which are now found to be

$\hat{C}^{\mathrm{c}}_{11}$	$\hat{C}^{\mathrm{c}}_{44}$	$\hat{C}^{\mathrm{c}}_{12}$
42.34	6.52	41.83

at the cubic phase and

$\hat{C}^{\mathrm{t}}_{11}$	$\hat{C}^{\mathrm{t}}_{33}$	$\hat{C}^{\mathrm{t}}_{44}$	$\hat{C}^{\mathrm{t}}_{66}$	$\hat{C}^{\mathrm{t}}_{12}$	$\hat{C}^{\mathrm{t}}_{13}$
44.37	42.32	6.52	6.52	39.81	41.83

at the tetragonal phase (compare with the values in (2) and (3) on page 6). This simple ansatz fits most moduli remarkably well, but fails to incorporate the symmetry breaking for $\hat{C}^{\mathrm{t}}_{44}$ and $\hat{C}^{\mathrm{t}}_{66}$ in the tetragonal phase.

To compare the Ericksen-James energy with the energy derived here, we include in Figure 5 two plots of sections of the Ericksen-James energy. The energy wells are relatively shallow. This difference becomes even more obvious if we analyse the energy's local behaviour around the cubic and tetragonal phase in the coordinate system $\bar{e}$. Transforming the elastic moduli of the Ericksen-James energy with the matrix M from Equation (6) gives

$$\begin{pmatrix} 0.507 & 0 & 0 \\ & 0.507 & 0 \\ & & 126 \end{pmatrix} \quad \text{and} \quad \begin{pmatrix} 0.507 & 0 & -0.019 \\ & 4.56 & 0 \\ & & 126 \end{pmatrix}$$

for $M^{-T}\hat{C}^{\mathrm{c}}M^{-1}$ and $M^{-T}\hat{C}^{\mathrm{t}}M^{-1}$ respectively.

A comparison with the expected values in Equations (7) and (8) shows that the cubic energy well is shallower by an order of magnitude in the $\bar{e}_1$-$\bar{e}_2$-plane, and so is the tetragonal minimum along $\bar{e}_1$. This is reflected in the simulations shown in Figure 6. In a two-dimensional setting, the dynamic equations of elasticity with capillarity and viscosity are approximated numerically, as described by Dondl and Zimmer [2004]. It is noticeable that the pattern formation is much more pronounced with the energy density derived here.

4.2 Cubic-to-monoclinic transition in CuZnAl

We wish to present an energy density for the cubic-to-monoclinic transition in CuZnAl for two reasons. Firstly, we are not aware of an explicit form for such an energy density in the literature, despite its importance for a numerical investigation of this phase transition. In itself, it is relevant for many applications. Falk and Konopka [1990] use a polynomial expansion to fit data for the cubic-to-monoclinic transition in CuAlNi. They show that this approach overestimates some elastic moduli in absolute value by more than an order of magnitude. Secondly, Zimmer [2004] observes that it is more difficult to describe the cubic-to-monoclinic transition than the cubic-to-tetragonal one using the orbit space approach. We present a way of deriving a phenomenological energy density that matches the elastic moduli of both phases. We start by a polynomial construction, in the vein of what is often called classical Landau theory. The simple polynomial expression we choose is not sufficient to fit all elastic moduli, and we thus augment the construction by splines defined on the orbit space.

4.2.1 Derivation of the phase coordinates

The cubic phase will again be considered as the reference configuration. Consequently, the coordinates of the cubic phase are again $e_1 = \cdots = e_6 = 0$. The elastic moduli are measured by Guenin et al. [1977]. We use their average value for $\hat{C}^{\mathrm{c}}_{11}$ and $\hat{C}^{\mathrm{c}}_{44}$ and the average value for $\frac{1}{2}\big(\hat{C}_{11} + \hat{C}_{12} + 2\hat{C}_{44}\big)$. The values in GPa are:

$\hat{C}^{\mathrm{c}}_{11}$	$\hat{C}^{\mathrm{c}}_{44}$	$\hat{C}^{\mathrm{c}}_{12}$
130	86	104

By cubic symmetry, we further have $\hat{C}^{\mathrm{c}}_{11} = \hat{C}^{\mathrm{c}}_{22} = \hat{C}^{\mathrm{c}}_{33}$, $\hat{C}^{\mathrm{c}}_{12} = \hat{C}^{\mathrm{c}}_{13} = \hat{C}^{\mathrm{c}}_{23}$, and $\hat{C}^{\mathrm{c}}_{44} = \hat{C}^{\mathrm{c}}_{55} = \hat{C}^{\mathrm{c}}_{66}$; all other moduli vanish.

The location of the monoclinic phase in the strain space is more difficult to locate, so we briefly sketch our derivation. The lattice constants of the monoclinic phase of $Cu_{68}Zn_{15}Al_{17}$ are well known;

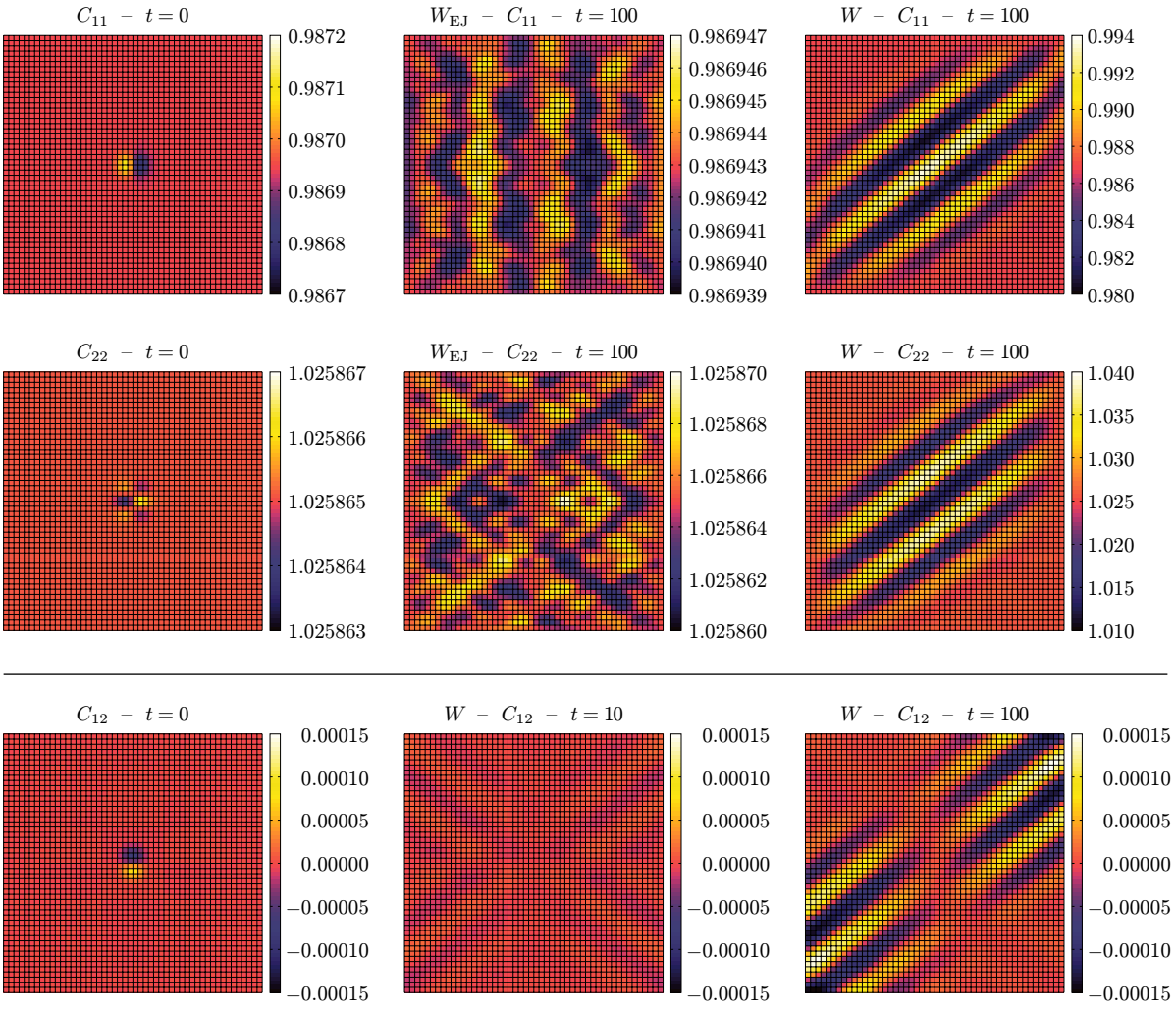

Figure 6: Results of two-dimensional finite-element simulations with two energy-densities for InTl. Top panel: Left: Values for C_{11} for the initial data. Middle: Snapshot after 100 time steps with a two-dimensional restriction of $W_{\mathrm{EJ}}(C)$ as given in (18). Right: Corresponding snapshot using the analogous two-dimensional restriction of the energy derived here. Note that the scale employed for $W_{\mathrm{EJ}}(C)$ ranges between 0.986939 and 0.986947, while the scale on the right varies between 0.980 and 0.994. For the relatively simple simulation employed here, pattern formation on the right (using the energy derived here) is obvious. There is no clear evidence for pattern formation using $W_{\mathrm{EJ}}(C)$ (middle); more sophisticated numerical procedures would be necessary to obtain a relaxation for $W_{\mathrm{EJ}}(C)$. Middle panel: Values for C_{22} analogously to the top panel. Note that the relaxation for the energy derived here exhibits oscillations in C_{22} which differ from those in C_{11} by a shift of about half a period (right). No such synchronization between C_{11} and C_{22} is evident for $W_{\mathrm{EJ}}(C)$ (middle). Bottom panel: Evolution of C_{12}, using the energy derived here. Left: start of the simulation, middle: after 10 time steps, right: after 100 time steps.

see Chakravorty and Wayman [1977]; Hane [1999]. We choose the values used by Rodriguez et al. [1993] for consistency, since the elastic moduli will also be taken from Rodriguez et al. [1993]. Thus, we use (data in Å) $a_0 = 5.996$ for the cubic parent phase, $a = 4.405$, $b = 5.34$ and $c = 38.2$ as lattice constants for the monoclinic cell, and $\delta = 88.4°$ as monoclinic angle.

Since there is an ambiguity in the choice of the martensitic unit cell, different descriptions of the cubic-to-monoclinic transformation in $Cu_{68}Zn_{15}Al_{17}$ exist. We follow the interpretation of Hane [1999]. See Bhattacharya [2003, Section 4.1 & Appendix] for another description. In practice, the differences between different theories are small.

Hane [1999] describes the cubic-to-monoclinic transition in $Cu_{68}Zn_{15}Al_{17}$ as a transition $DO_3 \to 18R$. The lattice correspondence between the two bases is

$$[100]_{18R} = [100]_{DO_3}, [010]_{18R} = [011]_{DO_3}, [001]_{18R} = [0\bar{1}1]_{DO_3}.$$

Thus, the correspondence matrix $DO_3 \to 18R$ is given by

$$\Delta = \begin{pmatrix} 1 & 0 & 0 \\ 0 & 1 & 1 \\ 0 & -1 & 1 \end{pmatrix}.$$

We decompose the cubic-to-monoclinic transformation into a cubic-to-tetragonal and a tetragonal-to-monoclinic one. Let us consider a cubic phase with lattice constant a_0, and a tetragonal phase with lattice constants a, b, c. Then the cubic-to-tetragonal Bain strain, expressed in 18R coordinates, is given by $B = \operatorname{diag}(\beta, \alpha, \gamma)$, with $\alpha = \sqrt{2}\frac{a}{a_0}$, $\beta = \frac{b}{a_0}$, $\gamma = \sqrt{2}\frac{c}{9a_0}$. This is the usual cubic-to-tetragonal Bain strain; compare, for example, Wayman [1964, Chapters 9 and 10]. The factor 9 takes the ration of the unit cells into account. A shear transforms the tetragonal phase into a monoclinic one; it is given by

$$S = \begin{pmatrix} 1 & 0 & 0 \\ 0 & 1 & \cos\delta \\ 0 & 0 & \sin\delta \end{pmatrix}.$$

The monoclinic phase, in 18R coordinates, is thus defined as $F_{18R} = SB$; in cubic (DO_3) coordinates, it becomes $F = \Delta^{-1} F \Delta$. Evaluating for the lattice parameters given above we obtain for $E = \frac{1}{2}(F^T F - \mathrm{Id})$

$$e_1^{\mathrm{m}} \approx -0.10342, \qquad e_2^{\mathrm{m}} \approx 0.00665, \qquad e_3^{\mathrm{m}} \approx 0.03574, \qquad e_4^{\mathrm{m}} \approx 0.03706, \qquad e_5^{\mathrm{m}} = e_6^{\mathrm{m}} = 0.$$

The elastic data for the monoclinic phase are fitted to data of Rodriguez et al. [1993]. We again take the average values of their measurements. Specifically, the values, in GPa, are as follows.

$\hat{C}^{\mathrm{m}}_{11}$	$\hat{C}^{\mathrm{m}}_{22}$	$\hat{C}^{\mathrm{m}}_{33}$	$\hat{C}^{\mathrm{m}}_{44}$	$\hat{C}^{\mathrm{m}}_{55}$	$\hat{C}^{\mathrm{m}}_{66}$	$\hat{C}^{\mathrm{m}}_{12}$	$\hat{C}^{\mathrm{m}}_{13}$	$\hat{C}^{\mathrm{m}}_{15}$	$\hat{C}^{\mathrm{m}}_{23}$	$\hat{C}^{\mathrm{m}}_{25}$	$\hat{C}^{\mathrm{m}}_{35}$	$\hat{C}^{\mathrm{m}}_{46}$
175	156	235	54	28	48	118	40	10	150	0	0	−10

The coordinate system needs to be changed to agree with the one used here. Thus, we consider the energy

$$W := \frac{1}{2}\int_\Omega \sum_{\alpha,\beta=1}^{6} \epsilon_\alpha C_{\alpha,\beta} \epsilon_\beta \,\mathrm{d}x, \tag{19}$$

where with the usual identification $\epsilon_\alpha = \epsilon_{jk}$ with $j, k \in \{1, 2, 3\}$,

$$\epsilon_{jk} = \frac{1}{2}\left(\frac{\partial u_j}{\partial x_k} + \frac{\partial u_k}{\partial x_j}\right) \text{ for } j \neq k \qquad \text{and} \qquad \epsilon_{jj} = \frac{\partial u_j}{\partial x_j}$$

The Lagrangian for Equation (19) gives the equations of motion,

$$\rho \ddot{u}_i = C_{ijkl} \frac{\partial^2 u_k}{\partial x_j \partial x_l},$$

which is the set of equations used to determine the elastic constants C_{ijkl} by Rodriguez et al. [1993]. Finally, the coordinates used by Rodriguez et al. [1993], here denoted with a subscript R, and those used by Hane [1999, Figure 3], are related as follows:

$$\begin{aligned}[100]_R &= [011]_{DO_3} = [010]_{18R},\\ [010]_R &= [100]_{DO_3} = [100]_{18R},\\ [001]_R &= [0\overline{1}1]_{DO_3} = [001]_{18R}.\end{aligned}$$

Thus, we transform the coordinates of the position and the deformation with the orthogonal matrix

$$\begin{pmatrix} 0 & 1 & 0 \\ \frac{\sqrt{2}}{2} & 0 & -\frac{\sqrt{2}}{2} \\ \frac{\sqrt{2}}{2} & 0 & \frac{\sqrt{2}}{2} \end{pmatrix}$$

into the DO_3-coordinates used here. The values, in GPa, turn out to be

$\hat{C}^{\mathrm{m}}_{11}$	$\hat{C}^{\mathrm{m}}_{22}$	$\hat{C}^{\mathrm{m}}_{33}$	$\hat{C}^{\mathrm{m}}_{44}$	$\hat{C}^{\mathrm{m}}_{55}$	$\hat{C}^{\mathrm{m}}_{66}$	$\hat{C}^{\mathrm{m}}_{12}$	$\hat{C}^{\mathrm{m}}_{13}$	$\hat{C}^{\mathrm{m}}_{14}$	$\hat{C}^{\mathrm{m}}_{23}$	$\hat{C}^{\mathrm{m}}_{24}$	$\hat{C}^{\mathrm{m}}_{34}$	$\hat{C}^{\mathrm{m}}_{56}$
156	117	122	370	46	56	67	67	−16	105.5	−32.5	−27.5	−3

4.2.2 Fitting the energy

As in Section 4.1, we split the energy in two parts,

$$W(e) := W_{\mathrm{d}}(e) + W_{\mathrm{o}}(e),$$

where W_{d} will be defined in the orbit spaces of the diagonal and the off-diagonal elements. As it turns out to be impossible to fit the difference between the moduli $\hat{C}^{\mathrm{m}}_{55}$ and $\hat{C}^{\mathrm{m}}_{66}$ with W_{d} and difficult to fit $\hat{C}^{\mathrm{m}}_{66}$, we match them with an appropriate energy W_{o}. To this end, we let

$$\begin{aligned}
\bar{\rho}_1 &:= \rho_1\rho_3 - \rho_8 &&= e_1{e_4}^2 + e_2{e_5}^2 + e_3{e_6}^2,\\
\bar{\rho}_2 &:= \rho_2\rho_3 - \rho_9 &&= {e_1}^2{e_4}^2 + {e_2}^2{e_5}^2 + {e_3}^2{e_6}^2,\\
\bar{\rho}_3 &:= ({\rho_3}^2 - \rho_6)/2 &&= {e_5}^2{e_6}^2 + {e_4}^2{e_6}^2 + {e_4}^2{e_5}^2,\\
\bar{\rho}_4 &:= \rho_3\rho_8 - \rho_{10} - \rho_1\bar{\rho}_3 &&= e_1{e_5}^2{e_6}^2 + e_2{e_4}^2{e_6}^2 + e_3{e_4}^2{e_5}^2,\\
\bar{\rho}_5 &:= \rho_3\rho_9 - \rho_{11} - \rho_2\bar{\rho}_3 &&= {e_1}^2{e_5}^2{e_6}^2 + {e_2}^2{e_4}^2{e_6}^2 + {e_3}^2{e_4}^2{e_5}^2
\end{aligned}$$

and make the ansatz

$$\begin{aligned}
W_{\mathrm{o}} := {} & \lambda_1\,(\rho_3{\lambda_4}^2 + 2\bar{\rho}_1\lambda_4 + \bar{\rho}_2) +\\
& \lambda_2\,(\bar{\rho}_3{\lambda_4}^2 + 2\bar{\rho}_4\lambda_4 + \bar{\rho}_5) +\\
& \lambda_3\,(\ 3{\lambda_4}^2 + 2\rho_1\lambda_4 + \rho_2)\,\rho_5
\end{aligned}$$

with indeterminate coefficients $\lambda_1, \ldots, \lambda_4$. Using

$$\mu_1 = \lambda_1 - \mu_2, \qquad \mu_2 = \frac{{\lambda_3}^2}{4\lambda_2}, \qquad \mu_3 = -2\frac{\lambda_2}{\lambda_3}, \qquad \mu_4 = \lambda_4,$$

the energy W_{o} can also be written as

$$\begin{aligned}
W_{\mathrm{o}} = {} & (e_1+\mu_4)^2\big(\mu_1{e_4}^2 + \mu_2(e_4 - \mu_3e_5e_6)^2\big) +\\
& (e_2+\mu_4)^2\big(\mu_1{e_5}^2 + \mu_2(e_5 - \mu_3e_4e_6)^2\big) +\\
& (e_3+\mu_4)^2\big(\mu_1{e_6}^2 + \mu_2(e_6 - \mu_3e_4e_5)^2\big),
\end{aligned} \tag{20}$$

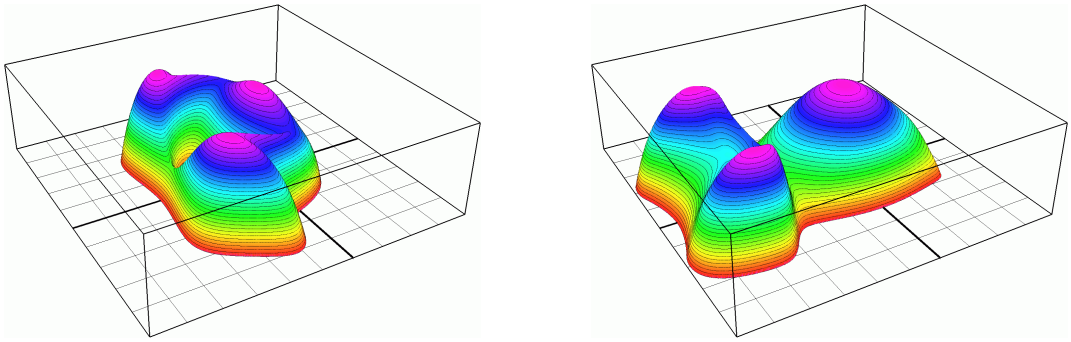

Figure 7: Energy in E-space, restricted to the planar cross-sections that contain the cubic phase e^{c} in the centre, the monoclinic phase e^{m} and either $(e_2^{\mathrm{m}}, e_1^{\mathrm{m}}, e_3^{\mathrm{m}}, e_5^{\mathrm{m}}, e_4^{\mathrm{m}}, e_6^{\mathrm{m}})$ (left) or $(e_1^{\mathrm{m}}, e_2^{\mathrm{m}}, e_3^{\mathrm{m}}, -e_4^{\mathrm{m}}, e_5^{\mathrm{m}}, e_6^{\mathrm{m}})$ (right). Note that we plot the negative energy to obtain a better view of the minima. The plots show the energy between 0 and 0.15.

which is obviously non-negative as long as $\mu_1 \geq 0$ and $\mu_2 \geq 0$. Moreover, W_{o} is zero at the cubic phase e^{c} and zero at the monoclinic phase e^{m} if we set

$$\mu_4 := -e_1^{\mathrm{m}} \approx 0.10342. \tag{21}$$

A straightforward calculation then reveals that by choosing

$$\mu_1 := 1149.96, \qquad \mu_2 := 4.8804, \qquad \mu_3 := 263.44, \tag{22}$$

the energy W_{o} fits the moduli $\hat{C}_{55}^{\mathrm{m}}$, $\hat{C}_{66}^{\mathrm{m}}$, and $\hat{C}_{56}^{\mathrm{m}}$.

We can now fit the remaining moduli conditions by constructing a function W_τ in the 4-dimensional orbit space τ that is spanned by the invariant polynomials

$$\tau_1 := \tilde{\rho}_1^{\mathrm{d}}, \qquad \tau_2 := \tilde{\rho}_2^{\mathrm{d}}, \qquad \tau_3 := \tilde{\rho}_3^{\mathrm{d}}, \qquad \tau_4 := \tilde{\rho}_1^{\mathrm{o}}$$

from Proposition 4 and Proposition 3, and finally setting $W_{\mathrm{d}} := W_\tau \circ \tau$. The ansatz

$$W_\tau(\tau_1, \tau_2, \tau_3, \tau_4) := \big(\hat{\tau} - \hat{\alpha}(\tau_2)\big)^T M \big(\hat{\tau} - \hat{\alpha}(\tau_2)\big) \cdot \omega(\tau_2) + \beta_2(\tau_2) + \beta_4(\tau_4) \tag{23}$$

with $\hat{\tau} := (\tau_1, \tau_3, \tau_4)^T$, $\hat{\alpha}\colon \mathbb{R} \to \mathbb{R}^3$, and $M \in \mathbb{R}^{3\times 3}$ then gives sufficient degrees of freedom to match all conditions. Similarly to the approach in Section 4.1, the energy W_τ is composed of a 3-dimensional hyperparaboloid in $\hat{\tau}$ with varying opening factor $\omega(\tau_2)$ whose minimum slides along the 3-dimensional path $\hat{\alpha} = (\alpha_1, \alpha_3, \alpha_4)^T$ and two profiles β_2 and β_4. We also need to keep in mind that the path must not leave the orbit space, in other words,

$$|\alpha_3(\tau_2)| \leq \sqrt{\tfrac{1}{2}|\tau_2|^3} \qquad \text{and} \qquad \alpha_4(\tau_2) \geq 0,$$

and construct $\hat{\alpha}$ accordingly. Again, we resorted to cubic B-splines for modelling the path, the profiles, and also the opening factor ω, as they provide sufficient flexibility for matching all conditions; see Appendix B for a detailed description. The resulting energy W is illustrated in Figure 7.

Analysing the stationary points of W is more difficult than for the energy in the previous section, because the gradients of W_{o} and W_{d} may cancel each other. In general, it does not suffice to examine them separately. The special case of $e_4 = e_5 = e_6 = 0$ can be analysed rather easily, as it is easy to see that $\mathrm{grad}(W_{\mathrm{o}})$ then vanishes. Moreover, as τ_4 and $\mathrm{grad}(\tau_4)$ are both zero in this situation, it follows that

$$\mathrm{grad}(W_\tau)(\tau_1, \tau_2, \tau_3, 0) = (0, 0, 0, *)$$

is sufficient for $\mathrm{grad}(W_{\mathrm{d}})$ to vanish. This condition is equivalent to

$$\det(\hat{M})\beta_2' = -\det(M)\alpha_4(2\omega\alpha_4' + \omega'\alpha_4), \tag{24}$$

where $\hat{M}$ is the upper left 2×2 submatrix of M. We can thus avoid spurious local minima by modelling ω, α_4, and β_2 such that Equation (24) never holds, which is not difficult to achieve by adjusting the control points of the corresponding B-splines.

In order to further verify the absence of other local minima, we implemented Newton's method, utilising the fact that we can derive both $\mathrm{grad}(W)$ and $\mathrm{Hess}(W)$ analytically for the above construction. We tested more than one million random initial positions. In each case the algorithm converged to the cubic phase, one of the monoclinic phases, or stopped at a saddle point.

5 Discussion

This paper is part of a sequence of papers, starting with [Zimmer, 2004]. The latter article provides the algebraic background (recalled here in Section 2 and derives the structure of the orbit space. Zimmer [2004], however, does not give any tools to fit energy functions to prescribed values. This matter is the topic of the present investigation. We decided to discuss the cubic-to-tetragonal transition and the cubic-to-monoclinic one. These examples have been chosen for their relevance in materials science. The cubic-to-tetragonal transition is discussed for InTl. The cubic-to-monoclinic example proves more challenging, and different ideas are used. To derive a specific energy, data is fitted for CuZnAl.

A key observation, already made by [Dondl and Zimmer, 2004], is that polynomials as global objects are not necessarily suitable to describe phase transitions: for lowest order invariant polynomials, the energy barrier is determined by elastic moduli even in the simplest case $a(\epsilon^2-1)^2$ describing two stable wells at $\pm\epsilon$. Higher order invariant polynomials result in steeply growing energies. Polynomials are proven to describe the local bifurcation picture correctly; in this sense, the framework developed in Section 3, describing the energy landscape by splines (piecewise polynomials) seems to be rather natural. We are not aware of any other systematic work in this direction (one may speculate that a possible reason could be that Landau developed his original idea of describing phase transformations by nonconvex energies before splines were invented).

We remark that these ideas not only apply to multiphase crystals, but also to much more complicated situations, for example, energetic landscapes arising in molecular dynamics. Applications of our ideas presented in that context will be an area of future research. Indeed, a very interesting recent finding by Tröster et al. [2005] is that the energy landscape for the ϕ^4 model exhibits, far from equilibrium, plateaus. Tröster et al. [2005] obtain these results by Wang-Landau simulations, and point out the deficiencies of polynomial interpolations in these regimes. If analyticity cannot be assumed in these regions, then the methods proposed here seem to be a suitable extension of Landau's original ideas.

Acknowledgements

Work for this article started while both authors were postdoctoral scholars at the California Institute of Technology. Progress continued during KH's research stay at the Max Planck Institute for Mathematics in the Sciences. We were fortunate to have James' manuscript [James, 1988] available. Sincere thanks are expressed to Patrick Dondl for running the simulations shown in Subsection 4.1. We thank Kaushik Bhattacharya for alerting us to experimental literature. We gratefully acknowledge the financial support of the US Air Force Office of Scientific Research through a MURI grant (F49620-98-1-0433), an NSF-ITR grant (ACI-0204932), the Deutsche Forschungsgemeinschaft through a post-doctoral grant (Ho 2457/1-1) (KH) as well as an Emmy Noether grant (Zi 751/1-1), and the EPSRC through an Advanced Research Fellowship (GR/S99037/1) (JZ).

A The energy for InTl

To simplify the reproduction of our results, we shall give a more detailed description of the energy that we construct in Section 4.1 to model the cubic-to-tetragonal transition in InTl. The overall temperature-dependent energy is given as

$$W(e,\theta) = W_{\mathrm{o}}(e) + W_\tau(\tau(e),\theta),$$

where the first term is

$$W_{\mathrm{o}} = 5.5\rho_3 - 815.253\rho_3\rho_2 + 3066860\rho_3{\rho_2}^2 - 5404.34\rho_9$$

with the invariant polynomials ρ_2, ρ_3, ρ_9 from Theorem 2. The second term is composed of the transformation

$$\tau = (\tau_1,\tau_2,\tau_2) = \big(\tilde\rho_1^{\mathrm{d}}, \tilde\rho_2^{\mathrm{d}}, \tilde\rho_3^{\mathrm{d}} - \tilde\rho_2^{\mathrm{d}}\sqrt{\tilde\rho_2^{\mathrm{d}}/2}\big)$$

with $\tilde\rho_1^{\mathrm{d}}$, $\tilde\rho_2^{\mathrm{d}}$, $\tilde\rho_3^{\mathrm{d}}$ from Proposition 4 and the energy

$$W_\tau(\tau,\theta) = (8826.43\tau_2 + 54.4)\big(\tau_1 - \alpha(\tau_2)\big)^2 + \beta(\tau_2,\theta) - 25.6600\tau_3.$$

The path α is defined as

$$\alpha(u) = 10^{-5}\cdot\sum_{i=1}^{3} a_i N_0^3(3944.77u - i)$$

with N_0^3 from Equation (1) and coefficients

$$a_1 = 1.33287, \qquad a_2 = 0, \qquad a_3 = -1.33287.$$

Finally, the temperature-dependent profile β is given by

$$\beta(u,\theta) = 10^{-5}\cdot\begin{cases}\displaystyle\sum_{i=-3}^{4} b_i(\theta)N_0^3(3944.77u - i) & \text{if } u < 0.0012675,\\ 3028.58u\theta + 10620.6u + 0.107273\theta - 11.6667 & \text{otherwise,}\end{cases}$$

with linearly varying coefficients

$$\begin{aligned} b_{-3}(\theta) &= 0.41303\theta - 131.11, & b_1(\theta) &= 2.36100\theta + 1.79487,\\ b_{-2}(\theta) &= -0.20652\theta + 22.46, & b_2(\theta) &= 3.17825\theta - 0.89744,\\ b_{-1}(\theta) &= 0.41303\theta + 41.27, & b_3(\theta) &= 3.94600\theta + 1.79487,\\ b_0(\theta) &= 1.37848\theta + 22.46, & b_4(\theta) &= 4.71374\theta + 4.48719. \end{aligned}$$

B The energy for CuZnAl

The energy that we introduced in Section 4.2 for the cubic-to-monoclinic transition in CuZnAl is given as the sum of two energies,

$$W(e) = W_{\mathrm{o}}(e) + W_\tau(\tau(e)).$$

As W_{o} is already described at full length by Equations (20)–(22), we are only concerned with the details of W_τ from Equation (23) here. The sliding hyperparaboloid is essentially a quadratic form, built from the positive definite symmetric matrix

$$M = \begin{pmatrix} 290.276 & 117.852 & -591.994\\ & 98461.3 & 6003.91\\ & & 67349.0 \end{pmatrix},$$

multiplied by the opening factor

$$\omega(u) = 0.0822047(1 - 92.8013u)^2 + 0.5.$$

The 3-dimensional path $\hat{\alpha}$ is composed of the three univariate functions

$$\alpha_j(u) = 10^{-5} \cdot \begin{cases} \sum_{i=0}^{3} a_{j,i} N_0^3(371.205u - i) & \text{if } u < 0.0107757, \\ A_{j,1}u + A_{j,0} & \text{otherwise,} \end{cases}$$

for $j \in \{1, 3, 4\}$ with coefficients

$$\begin{aligned} a_{1,0} &= 0, & a_{3,0} &= 0, & a_{4,0} &= 33.9803, \\ a_{1,1} &= -3508.62, & a_{3,1} &= -54.0341, & a_{4,1} &= 135.921, \\ a_{1,2} &= -3523.57, & a_{3,2} &= -65.3509, & a_{4,2} &= 137.344, \\ a_{1,3} &= -3538.51, & a_{3,3} &= -76.6676, & a_{4,3} &= 138.767, \\ A_{1,0} &= -3463.79, & A_{3,0} &= -20.0839, & A_{4,0} &= 131.652, \\ A_{1,1} &= -5547.24, & A_{3,1} &= -4200.83, & A_{4,1} &= 528.266. \end{aligned}$$

Finally, the path β_2 is given by

$$\beta_2(u) = 10^{-3} \cdot \begin{cases} \sum_{i=-3}^{4} b_{2,i} N_0^3(371.205u - i) & \text{if } u < 0.0134696, \\ 2337.81u - 27.2909 & \text{otherwise,} \end{cases}$$

with coefficients

$$\begin{aligned} b_{2,-3} &= -55.7158, & b_{2,-2} &= 10.3474, & b_{2,-1} &= 14.3263, & b_{2,0} &= 10.3474, \\ b_{2,1} &= 4.19860, & b_{2,2} &= -2.09930, & b_{2,3} &= 4.19860, & b_{2,4} &= 10.4965, \end{aligned}$$

and the path β_4 by

$$\beta_4(u) = 10^{-3} \sum_{i=-3}^{0} b_{4,i} N_0^3(2912.39u - i)$$

with coefficients

$$b_{-3} = -10.5234, \qquad b_{-2} = 0, \qquad b_{-1} = 10.5234, \qquad b_0 = 10.5234.$$

References

K. Bhattacharya. *Microstructure of Martensite. Why it forms and how it gives rise to the shape-memory effect.*, volume 2 of *Oxford Series on Materials Modelling*. Oxford University Press, 2003.

M. W. Burkart and T. A. Read. Diffusionless phase change in the Indium-Thallium system. *Transactions of the AIME*, 197(11):1516–1525, 1953.

S. Chakravorty and C. M. Wayman. Electron microscopy of internally faulted Cu-Zn-Al martensite. *Acta Metallurgica*, 25(9):585–601, 1977.

C. de Boor. *A Practical Guide to Splines*, volume 27 of *Applied Mathematical Sciences*. Springer, 2001.

P. Dierckx. *Curve and Surface Fitting with Splines*. Monographs on Numerical Analysis. Oxford University Press, 1993.

P. W. Dondl and J. Zimmer. Modeling and simulation of martensitic phase transitions with a triple point. *Journal of the Mechanics and Physics of Solids*, 52(9):2057–2077, 2004.

J. L. Ericksen. Some phase transitions in crystals. *Archive for Rational Mechanics and Analysis*, 73(2):99–124, 1980.

J. L. Ericksen. The Cauchy and Born hypotheses for crystals. In M. E. Gurtin, editor, *Phase Transformations and Material Instabilities in Solids*, pages 61–77. Academic Press Inc., 1984.

J. L. Ericksen. Constitutive theory for some constrained elastic crystals. *International Journal of Solids and Structures*, 22(9):951–964, 1986.

G. Fadda, L. Truskinovsky, and G. Zanzotto. Unified Landau description of the tetragonal, orthorhombic, and monoclinic phases of Zirconia. *Physical Review B*, 66:174107:1–10, 2002.

F. Falk and P. Konopka. Three-dimensional Landau theory describing the martensitic phase transformation of shape-memory alloys. *Zeitschrift für Physik B: Condensed Matter*, 2(1):61–77, 1990.

G. Farin. *Curves and Surfaces for CAGD.* Morgan Kaufmann Series in Computer Graphics and Geometric Modeling. Morgan Kaufmann, 5th edition, 2001.

R. J. Gooding, Y. Y. Ye, C. T. Chan, K. M. Ho, and B. N. Harmon. Role of non-symmetry-breaking order parameters in determining the martensitic energy barrier: The bcc-to-9R transformation. *Physical Review B*, 43(16):13 626–13 629, 1991.

G.-M. Greuel, G. Pfister, and H. Schönemann. Singular 2.0. A computer algebra system for polynomial computations. Technical report, Centre for Computer Algebra, University of Kaiserslautern, 2001.

G. Guenin, M. Morin, P. F. Gobin, W. Dejonghe, and L. Delaey. Elastic constant measurements in β Cu-Zn-Al near the martensitic-transformation temperature. *Scripta Metallurgica*, 11(12):1071–1075, 1977.

K. F. Hane. Bulk and thin film microstructures in untwinned martensites. *Journal of the Mechanics and Physics of Solids*, 47(9):1917–1939, 1999.

K.-H. Hellwege and A. M. Hellwege, editors. *Landolt-Börnstein. Numerical Data and Functional Relationships in Science and Technology*, volume 11 of *New Series. Group III: Crystal and Solid State Physics.* Springer, 1979.

R. D. James. Unpublished notes. 1988.

L. D. Landau. On the theory of phase transitions. In D. T. Haar, editor, *Collected papers of L. D. Landau.* Gordon and Breach Science Publishers, 1967.

A. E. H. Love. *A Treatise on the Mathematical Theory of Elasticity.* Dover Publications, 4th edition, 1944.

C. Procesi and G. Schwarz. Inequalities defining orbit spaces. *Inventiones Mathematicae*, 81(3):539–554, 1985.

P. L. Rodriguez, F. C. Lovey, G. Guenin, J. L. Pelegrina, M. Sade, and M. Morin. Elastic constants of the monoclinic 18R martensite of a Cu-Zn-Al alloy. *Acta Metallurgica et Materialia*, 41(11):3307–3310, 1993.

M. Rumberger. *Symmetrische dynamische Systeme: Differenzierbarkeit und linearisierte Stabilität.* PhD thesis, Universität Hamburg, Fachbereich Mathematik, 1997.

L. L. Schumaker. *Spline Functions: Basic Theory.* Krieger Publishing, 1993.

G. F. Smith and R. S. Rivlin. The strain-energy function for anisotropic elastic materials. *Transactions of the American Mathematical Society*, 88:175–193, 1958.

B. Sturmfels. *Algorithms in Invariant Theory.* Springer, 1993.

J.-C. Tolédano and P. Tolédano. *The Landau Theory of Phase Transitions.* World Scientific Publishing, 1987.

A. Tröster, C. Dellago, and W. Schranz. Free energies of the ϕ^4 model from Wang-Landau simulations. *Physical Review B*, 72(9):094103–1–11, 2005.

C. M. Wayman. *Introduction to the Crystallography of Martensitic Transformations.* Macmillan Series in Materials Science. The Macmillan Company, 1964.

A. S. Wineman and A. C. Pipkin. Material symmetry restrictions on constitutive equations. *Archive for Rational Mechanics and Analysis*, 17:184–214, 1964.

J. Zimmer. Stored energy functions for phase transitions in crystals. *Archive for Rational Mechanics and Analysis*, 172(2):191–212, 2004.